Polar Research

RESEARCH/REVIEW ARTICLE

Eruption age of the Sverrefjellet volcano, Spitsbergen Island, Norway

Allan H. Treiman

Lunar and Planetary Institute, 3600 Bay Area Boulevard, Houston, TX 77058, USA

Keywords
Svalbard; Spitsbergen; basalt; Knipovich Ridge; Ar–Ar.

Correspondence
Allan H. Treiman, Lunar and Planetary Institute, 3600 Bay Area Boulevard, Houston, TX 77058, USA.
E-mail: treiman@lpi.usra.edu

Abstract

Sverrefjellet is a Pleistocene-age basaltic volcanic construct on north-western Spitsbergen Island (Svalbard Archipelago, Norway). Published ages for the Sverrefjellet eruption range between 6000 years and ca. 1 million years before present. The age of eruption is dated here as 1.05 ± 0.07 (1σ) My, consistent with Ar–Ar isochron and plateau ages of several analysed samples. Radiogenic Ar represents a small proportion of the released Ar, $<15\%$ in nearly all samples. Non-radiogenic Ar components include air, excess ^{40}Ar (seen as inverse isochron intercept values $> {}^{40}Ar/{}^{36}Ar = 295.5$), low-temperature alterations (Ar release at low temperature, with high Cl/K), carbonates and zeolites (Ar release at intermediate temperature) and xenolithic material (Ar release at high temperature, high Ca/K). The effects of the largely non-radiogenic argon sources are also seen in the total-gas Ar–Ar "ages", which range from 1.3 to 10.3 My, significantly larger than the inferred eruption age. It is likely that total-gas Ar–Ar "ages" and whole-rock K–Ar "ages" of similar basalts also exceed their true eruption ages.

To access the supplementary material to this article please see Supplementary files under Article Tools online.

In north-western Spitsbergen, near the fjords Bockfjorden and Woodfjorden, there are several Quaternary-age volcanic extrusive constructs and subvolcanic pipes of alkaline olivine basalt (Fig. 1). Sverrefjellet is the most accessible and widely known of these volcanoes, in part because of its abundant mantle xenoliths (Amundsen et al. 1987; Ionov et al. 1996; Kopylova et al. 1996). The ages of Sverrefjellet and the other volcanoes are tectonically important, as they represent off-axis eruptions associated with the Knipovich mid-ocean ridge (Crane et al. 2001; Sushchevskaya et al. 2008). These volcanoes and several active hot springs sit along, or near, the Breibogen–Bockfjorden fault system (Evdokimov 2000; Jamtveit et al. 2006; Salvigsen & Høgvard 2007), which runs along Bockfjorden, and extends south to Isfjorden (near Longyearbyen) and north offshore onto the Yermak Plateau (Fig. 1a; Crane et al. 2001). Current motion on the Breibogen fault system is extensional, both from local observations and a regional perspective (Crane et al. 2001).

The ages of these alkaline volcanic centres are poorly known, with radiogenic isotope and stratigraphic values ranging from Holocene to >2 My. Semevskij (1965) suggested that Sverrefjellet erupted in the mid-Holocene, 6–10 Ky; such a young, post-glacial age is inconsistent both with the presence of glacial erratics at the summit of Sverrefjellet (Skjelkvåle et al. 1989) and the presence of older shell fragments on a beach terrace cut into Sverrefjellet (Salvigsen & Høgvard 2005). From geomorphology and the presence of glacial erratics, Skjelkvåle et al. (1989) inferred that Sverrefjellet erupted during the last interglacial, between 100 and 250 Ky. Burov and Zagruzina (1976) give a whole-rock K–Ar age of 1 ± 0.5 My for Sverrefjellet. Whole-rock K–Ar ages for nearby alkaline volcanoes Sigurdfjellet and Halvdanpiggen are ca. 2.7 and ca. 2.0 My, respectively

Citation: *Polar Research* 2012, *31*, 17320, DOI: 10.3402/polar.v31i0.17320

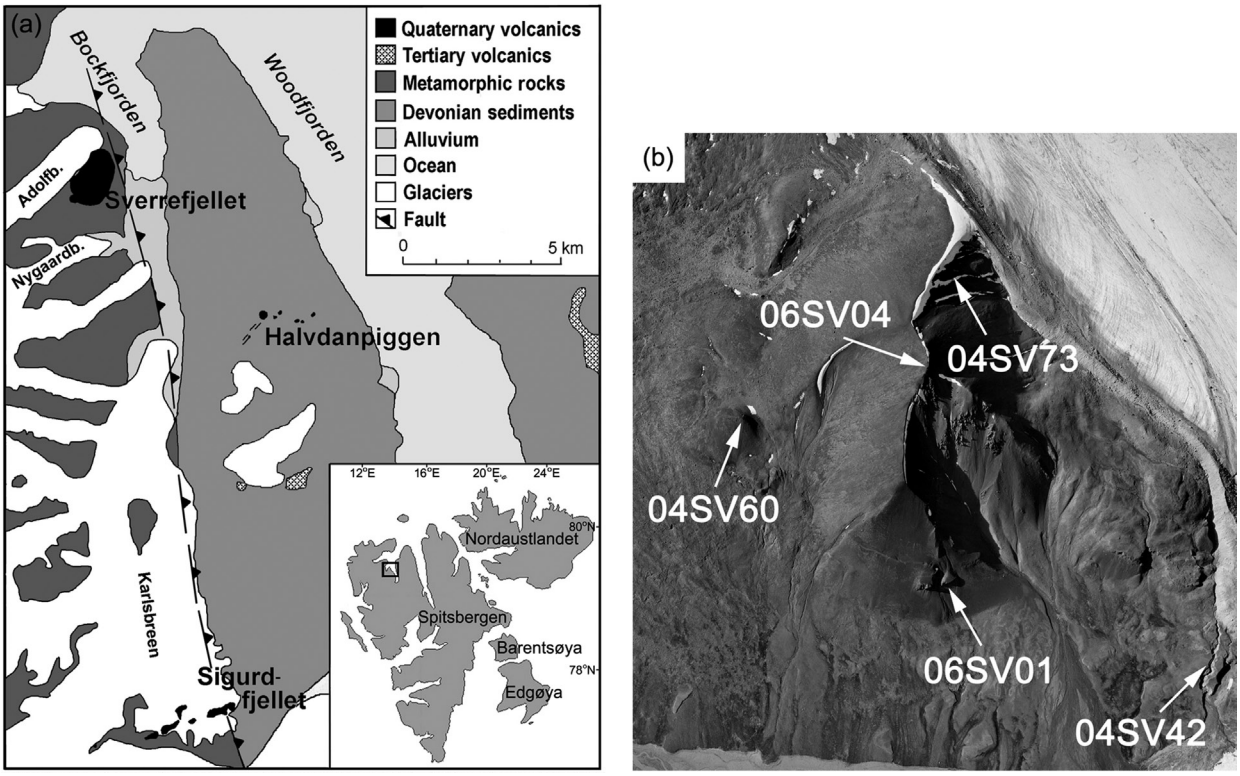

Fig. 1 Geology of the Sverrefjellet area and sample locations. (a) Simplified geological map of the area including Bockfjorden, Sverrefjellet and Woodfjorden, with locations and names of major Quaternary igneous bodies (after Skjelkvåle et al. 1989). North is to the top. The small square on the inset shows location of the investigated area on Spitsbergen. (b) Aerial photograph of Sverrefjellet, annotated with sample locations. North is to the right and the scene is ca. 3 km across. Adolfbreen glacier is at the upper right; alluvium in Bockfjorden is at the bottom of image. The base image is aerial photograph S70-2558, from the Norwegian Polar Programs office.

(Evdokimov et al. 1991; Kopylova et al. 1996; Evdokimov 2000; Sushchevskaya et al. 2008). Skjelkvåle et al. (1989) cite unpublished Ar–Ar plateau ages of 1.5–2 My for mantle xenocrysts (kaersutite, anorthoclase and biotite) from Sverrefjellet, Sigurdfjellet and Halvdanpiggen; these data are an upper bound to the age(s) of the Sverrefjellet basalts.

In this study, I focus on the eruption age of the Sverrefjellet volcano, a conical peak ca. 500 m tall, on the west side of Bockfjorden (Fig. 1; Skjelkvåle et al. 1989; Evdokimov 2000). The summit of Sverrrefjell is at 79.431°N, 13.305°E, with an elevation of ca. 510 m above average sea level, based on global positioning system measurements (E. Hausrath, pers. comm.). The steep east face of Sverrefjellet abuts Bockfjorden and its deposits of glacial outwash (Fig. 1). That east face is parallel to Bockfjorden, suggesting that it was eroded during an ancient advance of the Karlsbreen glacier (now south of Bockfjorden). Several wave-cut terraces are preserved on the east face of Sverrefjellet and are truncated by Vulkanbekken, a small stream valley that drains the east side of Sverrefjellet into Bockfjorden. The northern side of Sverrefjellet is against and parallel to the Adolfbreen glacier and its moraines, suggesting that earlier advances of Adolfbreen carved away some of the original volcano. The south side of Sverrefjellet slopes gently down to a low plain north of the Nygaardbreen glacier (Fig. 1).

Sverrefjellet is composed mostly of basalt cinders, with outcrops of basaltic pillow lavas, dikes and pipes (Skjelkvåle et al. 1989). Pillow lavas are present in scattered locales and elevations on the south, east and north faces of the volcano. Dikes are exposed on the east, north-east and west faces, and the east face also exposes many vertical lava pipes or tubes. Lithified volcaniclastics are found only in a few exposures on the lower east slopes. All of the basalts of Sverrefjellet contain abundant xenoliths of mantle peridotites and Caledonian-age metamorphic rocks (Amundsen et al. 1987; Skjelkvåle et al. 1989; Ionov et al. 1996; Kopylova et al. 1996).

Citation: *Polar Research* 2012, *31*, 17320, DOI: 10.3402/polar.v31i0.17320

Table 1 Sample data: analysed basalts. See Fig. 1 for exact sample locations.

Sample	Location	Elevation (m)	Rationale
04SV42	Stream cut, NE apron, below glacial sediments	30	Glassy rind of pillow or pillow fragment.
04SV60	Knob S of summit	346	Glassy outer rind of pillow, kms south of other samples
04SV73	N slope, highest outcrops of pillow basalt	430	Glassy rind of pillow, highest exposure of pillow basalt.
06SV01A	Cliffs exposing pillow basalts on W slope	130	Glassy rind of pillow, ca. 4 m diameter. Few small vesicles
06SV01B	Cliffs exposing pillow basalts on W slope	130	Mid-section of above pillow, with large vesicles
06SV01C	Cliffs exposing pillow basalts on W slope	130	Interior of above pillow, next to lava tube at core of pillow. More crystalline, with small vesicles.
06SV04	Summit of Sverrefjellet	510	Basalt dike exposed at summit. Mostly crystalline.

Samples and methods

Samples

The samples analysed in this study (Table 1) were collected during the 2004 and 2006 expeditions of the Arctic Mars Analogue Svalbard Expedition consortium (Steele et al. 2007). These samples included the freshest, least-altered samples found in place and were chosen from across the whole volcano, from a knob in the south (4SV60) to the northernmost rock in place (pillow lava 04SV42), and from the lowest solid rock exposure (04SV42) to the highest pillow lava (04SV73) and the volcano's summit (06SV04).

Ar–Ar age determination

Argon isotope analyses and age determination followed methods similar to those of Hall et al. (2004). Whole-rock samples were broken into ca. 1-mm fragments, and those without visible alteration or xenolithic material were selected for analyses. These fragments were wrapped in pure Al foil and loaded into fused silica tubes for neutron irradiation. Irradiation of samples, standards and controls were done simultaneously at site 5C at McMaster University, for 1 h (3 MWhr). Samples and standards were analysed using an argon ion continuous laser fusion system with a maximum power of 5 W, operating in multiline mode. Step heating was performed by shining a defocused laser beam, and samples consisted of 5 ca. 1–2-mm diameter rock pieces that were individually heated for 30 s for each gas fraction release. The released gas was purified using an LN_2 cold trap and two 10 l s^{-1} ST-101 getter pumps (SAES Getters, Lainate, Italy). After a total isolation time of 3 min, the gas was let into a VG 1200S Mass Spectrometer (VG Analytical/Micromass Ltd, Manchester, UK) operating at 150 mA emission current that is equipped with a Faraday and Daly detector. Each Ar isotope was measured 12 times, and isotope measurements were extrapolated to inlet time. The Daly detector was used for all runs, except those in which an excessively strong signal required use of the Faraday detector. In these cases, a gain value for the Daly was measured either during or at the end of the run. Mass discrimination of the entire source-detector system was monitored daily using 3×10^{-9} ml standard temperature and pressure (STP) of air Ar and correcting the measured ^{40}Ar to ^{36}Ar ratio to 295.5. Laser fusion system inlet blanks were monitored once every five steps, and typical blank levels were 2×10^{-14}, 4×10^{-14}, 1×10^{-14}, 4×10^{-14} and 5×10^{-12} ml STP for masses $36-40$, respectively. The rate of increase at mass 40 was typically 6×10^{-13} ml STP per min. Ar isotope measurements were corrected for decay of ^{37}Ar and ^{39}Ar, plus the build-up of ^{36}Ar from the decay of ^{36}Cl and interfering nuclear reactions from Ca and K. Sample isotope values are blank corrected. Samples were interspersed with standard mineral flux monitor packets, and the "J" parameters measured at each standard position were interpolated to generate functions, which return the "J" value for any sample's position for each irradiation. Ages were calibrated against the standard Fish Canyon biotite FCT-3 (Hall & Farrell 1995) and adjusted to the recalibrated age of the Fish Canyon sanidine (28.305 ± 0.036 My; Renne et al. 2010). Uncertainties for total-gas, plateau and isochron ages were obtained with standard methods; statistics on inverse isochrons were calculated with the code Isoplot 3.72, by K. Ludwig (University of California, Berkeley). The uncertainties include error estimates for the measured value of "J" (including those of individual standards, the "J" function parameters and scatter of "J" measurements about the fitted function) but do not include the ca. 2% uncertainty in the apparent age of the FCT-3 standard (Dazé et al. 2003).

Two splits of each sample were analysed, in separate irradiations; splits are labelled "a" and "b". The replicate splits commonly had distinctly different release patterns (see Supplementary Appendix).

Table 2 Ar–Ar ages. See Fig. 2. Uncertainties are 1σ.

Sample	Plateau age[a] (My)	MSWD[b]	Isochron age[c] (My)	MSWD	Isochron $^{40}Ar/^{36}Ar$(i)	Total-gas age (My)
04SV42a	0.62±0.07	1.64	1.27±0.11	0.96	285.6±1.9	1.4
04SV42b	1.10±0.07	1.49	None	–	–	2.3
04SV60a	1.02±0.04	1.79	1.17±0.08	1.4	292.3±1.7	1.3
04SV60b	1.14±0.06	1.92	0.99±0.08	1.8	299.6±2.3	1.4
04SV73a	1.05±0.07	1.45	0.86±0.09	0.94	298.9±2.3	1.4
04SV73b	1.42±0.06	1.90	1.05±0.07	1.19	300.8±1.5	1.6
06SV01Aa	None	–	None	–	–	2.3
06SV01Ab	1.38±0.06	1.57	1.61±0.10	0.75	282.8±4.8	1.8
06SV01Ba	None	–	None		–	10.4
06SV01Bb	None	–	None	–	–	3.4
06SV01Ca	1.04±0.07	0.54	0.89±0.65	0.58	297.0±4.8	1.9
06SV01Cb	None	–	None	–	–	1.5
06SV04a	None	–	None	–	–	5.3
06SV04b	None	–	None	–	–	3.3

[a]Assumes a single non-radiogenic component of $^{40}Ar/^{36}Ar$ = 295.5 (see Supplementary Appendix).

[b]Mean square weighted deviation.

[c]Generally exclude first four, and last two, thermal release steps (see Supplementary Appendix).

Results

Summary Ar − Ar results are given in Table 2, which includes release plateau ages, isochron ages, $^{40}Ar/^{36}Ar$ of non-radiogenic argon (assuming two-component mixing) and total-gas ages; the full dataset is tabulated in the Supplementary Appendix. Figure 2 shows data for selected samples: Ar–Ar ages, Ca/K and Cl/K for each heating step of the analyses and inverse isochron graphs of the Ar–Ar data.

The Ar–Ar ages of the Sverrefjellet samples with recognizable plateaus or isochrons are all in the vicinity of a million years, roughly consistent with earlier K–Ar ages but not consistent with inferences from stratigraphy or geomorphology. The most likely age of the eruption is 1.05 ± 0.07 (1σ) My (mean square weighted deviation = 1.9), which is the uncertainty-weighted mean of the following ages (Table 2): inverse isochron ages for 04SV42a, 04SV60b and 04SV73b (samples with $^{40}Ar/^{39}Ar$(i) different from air); and plateau ages of 04SV42b, 04SV60a, 04SV73a and 06SV01Ca (samples with $^{40}Ar/^{39}Ar$(i) closer to that of air). Ar–Ar plateau ages range from 0.6 to 1.4 My, and isochron ages range from 0.9 to 1.6 My (Table 2). This range of results reflects, in part, uncertainty because of the small proportions of radiogenic argon in the Sverrefjellet samples—no thermal release step contains more than 50% radiogenic ^{40}Ar, and most contain <15%.

Several non-radiogenic Ar components are evident in release spectra and isochrons. Almost all Ar release spectra show higher apparent ages and increased Cl/K in the lowest temperature steps (Fig. 2a–c); these probably represent gas from alteration materials like clays and sideromelane. A few samples show high apparent ages in middle temperature release steps (Fig. 2d), and they likely represent gas released during decomposition of carbonates and zeolites (Treiman et al. 2002). Many release spectra show high apparent ages and elevated Ca/K in the highest temperature release steps (Fig. 2a, d); these probably represent gas from crustal xenoliths (Caledonian age) or mantle xenoliths (K–Ar ages of 1.5–2 My; Skjelkvåle et al. 1989). Several isochron plots are consistent with a non-radiogenic argon component with $^{40}Ar/^{36}Ar$ of ca. 300, significantly above that of air, 295.5 (Fig. 2c). This excess ^{40}Ar may be ascribed to incomplete degassing of the basalt lava on eruption and/or entrapment of ^{40}Ar released from xenoliths and xenocrysts.

Given these sources of excess ^{40}Ar, it is not surprising that the total-gas Ar–Ar ages for the samples are greater

Fig. 2 Ar–Ar thermal release spectrum and isochron graphs for selected samples. See Fig. 1 and Table 1 for locations and the Supplementary Appendix for full data. In the thermal release spectra, statistically significant age plateaus are shown by horizontal arrows; ''f39'' is the fraction of ^{39}Ar release included in the plateau. Ca/K and Cl/K are also shown. Mean square weighted deviation is abbreviated as MSWD. The lower graphs are inverse isochron plots; the x-intercept is inversely proportional to sample age (see Table 2); and the y-intercept is the $^{36}Ar/^{40}Ar$ ratio of a non-radiogenic component (see Table 2). Solid lines are isochrons for selected release steps (generally excluding the lowest four and highest two steps); dashed lines are regressed through the whole dataset. Figures (a) and (b) are for splits of the same rock sample; (b) has identical plateau and isochron ages and a trapped $^{40}Ar/^{36}Ar$ consistent with air. The sample of (c) has an isochron age consistent with those of (a) and (b), but a trapped $^{40}Ar/^{36}Ar$ higher than air; hence, its calculated plateau age exceeds its isochron age. The sample of (d) shows no isochron or Ar release plateau. Its Ar is dominated by releases in the middle heating steps, probably from decomposition of carbonates and/or zeolites.

Citation: *Polar Research* 2012, *31*, 17320, DOI: 10.3402/polar.v31i0.17320

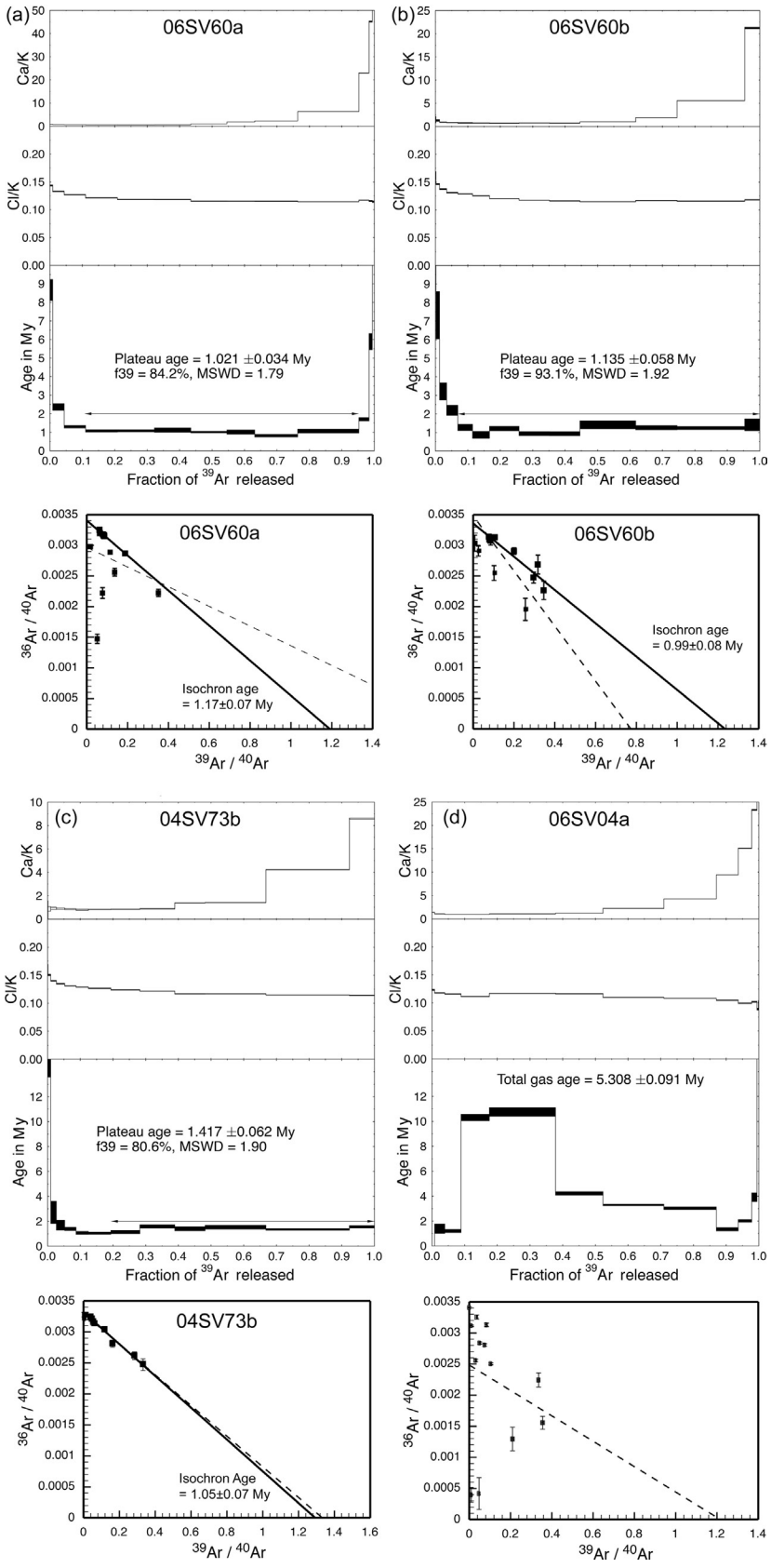
(a)
06SV60a
Ca/K
Cl/K
Age in My
Plateau age = 1.021 ±0.034 My
f39 = 84.2%, MSWD = 1.79
Fraction of 39Ar released
(b)
06SV60b
Plateau age = 1.135 ±0.058 My
f39 = 93.1%, MSWD = 1.92
06SV60a
36Ar / 40Ar
Isochron age
= 1.17±0.07 My
39Ar / 40Ar
06SV60b
Isochron age
= 0.99±0.08 My
(c)
04SV73b
Plateau age = 1.417 ±0.062 My
f39 = 80.6%, MSWD = 1.90
(d)
06SV04a
Total gas age = 5.308 ±0.091 My
04SV73b
Isochron Age
= 1.05±0.07 My

than plateau or isochron ages and range from 1.4 to 10 My (Table 2).

Conclusions

The Ar–Ar age data here give the eruption age of Sverrefjellet as 1.05 ± 0.07 (1σ) My, (Table 2), which is consistent with the single literature K–Ar age of 1 ± 0.5 My (Burov & Zagruzina 1976). Eruption at 1.05 Mya means that Sverrefjellet, as a landform, has survived several glaciations and interglacials. Traces of this complex history are preserved in its geomorphology, which is currently under investigation.

The Ar–Ar data in this study define the ages of the Sverrefjellet volcano and help restrict the possible ages of related basaltic rocks in the area. For the Sverrefjellet rocks, total-gas ages are always greater than plateau or isochron ages of eruption (Table 2) because of the several components of excess ^{40}Ar. Similarly, whole-rock K–Ar ages ought to be equal to or greater than eruption ages. The published K–Ar ages for the Sigurdfjellet and Halvdanpiggen volcanoes, ca. 2 and ca. 2.7 My, respectively (Evdokimov et al. 1991), must therefore be considered upper limits to eruption ages, as rocks of those volcanos contain the same potential sources of excess ^{40}Ar as do the rocks of Sverrefjellet: mantle xenoliths and megacrysts, crustal xenoliths, secondary minerals and low-temperature alterations (Amundsen et al. 1987; Skjelkvåle et al. 1989; Treiman et al. 2002). It is not known if these other Quaternary eruptions were contemporaneous with Sverrefjellet, and their tectonic significance (e.g., Vågnes & Amundsen 1993; Crane et al. 2001) will be clarified as their eruption ages become known with more certainty.

Acknowledgements

Samples were collected with assistance from H.E.F. Amundsen, E. Hausrath and D. Blake. Sverrefjellet was visited and sampled on several Arctic Mars Analogue Svalbard Expeditions, for which I am grateful to H.E.F. Amundsen, A. Steele, the US National Aeronautics and Space Administration's Astrobiology Science & Technology for Exploring Planets (NASA ASTEP) programme and the Governor of Svalbard. I am also grateful to D. Bogard for helpful discussions and to K. Ludwig (University of California, Berkeley) for sharing his Isoplot 3.72 code. C.M. Hall (University of Michigan) performed the Ar–Ar analyses and assisted with data analysis. This work was supported in part by a subcontract to the author under NASA ASTEP grant no. NNG06GB31C (Dr A. Steele, principal investigator). Reviews by C.M. Hall, A.A.P. Koppers, P. van den Bogaard and an anonymous reviewer were extremely helpful. This publication is Lunar and Planetary Institute contribution no. 1657.

References

Amundsen H.E.F., Griffin W.L. & O'Reilly S.Y. 1987. The lower crust and upper mantle beneath northwest Spitsbergen: evidence from xenoliths and geophysics. *Tectonophysics 139*, 169–185.

Burov J.P. & Zagruzina I.A. 1976. Resul'taty opredelenija absoljutnogo vozrasta kajnozojskih bazitov severnoj časti o. Špicbergen. (Results of a determination of the absolute age of Cenozoic basic rocks of the northern part of the island of Spitsbergen.) In V.N. Sokolov (ed.): *Geologija Sval'barda.* (*The geology of Svalbard.*) Pp. 139–140. Leningrad: Scientific Research Institute of Arctic Geology.

Crane K., Doss H., Vogt P., Sundvor E., Cherkashov G., Poroshina I. & Joseph D. 2001. The role of the Spitsbergen shear zone in determining morphology, segmentation and evolution of the Knipovich Ridge. *Marine Geophysical Researches 22*, 153–203.

Dazé A., Lee J.K.W. & Villeneuve M. 2003. An intercalibration study of the Fish Canyon sanidine and biotite ^{40}Ar/^{39}Ar standards and some comments on the age of the Fish Canyon Tuff. *Chemical Geology 199*, 111–127.

Evdokimov A.N. 2000. *Vulkany Špicbergena.* (*Volcanoes of Spitsbergen.*) St. Petersburg: All-Russian Research Institute for Geology and Mineral Resources of the World Ocean.

Evdokimov A.N., Germanov E.V., Daševskaja D.M. & Genšaft J.S. 1991. *Kajnozojskij magmatizm, gidrotermal' naja dejatel'nost' i perspektivy rudonosnosti zony razlomov Ekman-fiord–Vud-fiord, ostrov Zapadnyj Špicbergen. (Cenozoic magmatism, hydrothermal activity and ore potential of Ekmanfjorden and Woodfjorden fault zone, Spitsbergen.)* Leningrad: PGO Sevmorgeologija.

Hall C.M. & Farrell J.W. 1995. Laser ^{40}Ar/^{39}Ar ages of tephra from Indian Ocean deep-sea sediments: tie points for the astronomical and geomagnetic polarity time scales. *Earth and Planetary Science Letters 133*, 327–338.

Hall C.M., Kesler S.E., Russell N., Piñero E., Sanchez R., Perez M., Moreira J. & Borges M. 2004. Age and tectonic setting of the Camagüey volcanic-intrusive arc, Cuba: late cretaceous extension and uplift in the western Greater Antilles. *Journal of Geology 112*, 521–542.

Ionov D.A., O'Reilly S.Y., Genshaft Y.S. & Kopylova M.G. 1996. Carbonate-bearing mantle peridotite xenoliths from Spitsbergen: phase relationships, mineral compositions, and trace element residence. *Contributions to Mineralogy and Petrology 125*, 375–392.

Jamtveit B., Hammer Ø., Andersson C., Dysthe D.K., Heldmann J. & Fogel M.L. 2006. Travertines from the Troll thermal springs, Svalbard. *Norwegian Journal of Geology 86*, 387–395.

Citation: *Polar Research* 2012, *31*, 17320, DOI: 10.3402/polar.v31i0.17320

Kopylova M.G., Genshaft Y.S. & Dashevskaya D.M. 1996. Petrology of upper mantle and lower crustal xenoliths from northwestern Spitsbergen. *Petrology 4*, 493–518.

Renne P.R., Mundil R., Balco G., Min K. & Ludwig K.R. 2010. Joint determination of ^{40}K decay constants and ^{40}Ar*/^{40}K for the Fish Canyon sanidine standard, and improved accuracy for ^{40}Ar/^{39}Ar geochronology. *Geochimica et Cosmochimica Acta 74*, 5349–5367.

Salvigsen O. & Høgvard K. 2005. Glacial history, Holocene shoreline displacement and palaeoclimate based on radiocarbon ages in the area of Bockfjorden, north-western Spitsbergen, Svalbard. *Polar Research 25*, 15–24.

Salvigsen O. & Høgvard K. 2007. Gygrekjelda, a new warm spring in Bockfjorden, Svalbard. *Polar Research 27*, 107–109.

Semevskij D.V. 1965. K voprosu o vozraste vulkana Sverre. (Age of the Sverrefjellet volcano.) In V.N. Sokolov (ed.): *Materialy po geologii Špicbergena. (The geology of Spitsbergen.)* Pp. 272–275. Leningrad: Scientific Research Institute of Arctic Geology.

Skjelkvåle B.-L., Amundsen H.E.F., O'Reilly S.Y., Griffin W.L. & Gjelsvik T. 1989. A primitive alkali basaltic stratovolcano and associated eruptive centers, northwestern Spitsbergen: volcanology and tectonic significance. *Journal of Volcanology and Geothermal Research 37*, 1–19.

Steele A., Amundsen H.E.F., Botta O. & The AMASE 2006. Team. 2007. The Arctic Mars Analogue Svalbard Expedition 2006. In G. Groemer (ed.): *Mars2030—AustroMars Science Workshop. Proceedings of the conference held in at the University of Salzburg, 24–26 September*. Pp. 55–61. Vienna: Austrian Space Forum.

Sushchevskaya N.M., Evdokimov A.N., Belyatsky B.V., Maslov V.A. & Kuz'min D.V. 2008. Conditions of quaternary magmatism at Spitsbergen Island. *Geochemistry International 46*, 1–16.

Treiman A.H., Amundsen H.E.F., Blake D.F. & Bunch T. 2002. Hydrothermal origin for carbonate globules in Martian meteorite ALH84001: a terrestrial analogue from Spitsbergen (Norway). *Earth and Planetary Science Letters 204*, 323–332.

Vågnes E. & Amundsen H.E.F. 1993. Late Cenozoic uplift and volcanism on Spitsbergen: caused by mantle convection? *Geology 21*, 251–254.